A Resetting Observer for Linear Time-Varying Systems With Application to Dynamic Positioning of Marine Surface Vessels

Tobias R. Torben, Andrew R. Teel, *Fellow, IEEE*, Øivind K. Kjerstad, Emilie H. T. Wittemann, and Roger Skjetne, *Senior Member, IEEE*

***Abstract*— This brief presents a resetting observer for linear time-varying (LTV) systems. The motivation for the observer is better handling of unmodeled dynamics and reactiveness to external disturbances without compromising steady-state performance. A reset is triggered if the output estimation error exceeds predefined bounds. The proposed observer uses a finite-time observer (FTO) approach to calculate corrected state estimates after a reset is triggered. The FTO equations are derived for LTV systems, and a method for calculating the state transition matrices online is presented. The observer equations are formulated in a hybrid dynamical systems framework, and sufficient conditions for uniform global preexponential stability are given. The method is applied to observer design for dynamic positioning (DP) of marine surface vessels. Numerical simulations as well as model scale experiments of this application show promising results, with improved transient performance compared to state-of-the-art observers.**

***Index Terms*— Dynamic positioning (DP), finite-time observers (FTOs), hybrid dynamical systems, linear time-varying (LTV) systems, marine surface vessels, observer design.**

I. Introduction

OBSERVERS play a vital role in control systems. The main objective of an observer is to estimate the states of a system based on partial and uncertain measurements. Also, an observer may have a signal processing role, where it filters noise and unwanted frequency components before the signal enters the control loop. Dynamic positioning (DP) of a marine vessel is the process of automatic position and heading control by dynamically controlling the thrusters [1]. The model-based nonlinear passive observer (NPO) of [2] is state-of-the-art in industrial DP systems. The NPO takes only uncertain pose measurements as input and estimates pose, velocity, and a bias load. A challenge for the NPO is to handle unmodeled dynamics and external time-varying disturbances in a reactive manner, without using too high injection gains causing measurement noise to be amplified and unwanted oscillations to occur in the state estimates. Addressing this challenge has the potential to enhance the transient behavior of the control system and reduce fuel consumption.

Several applications today call for DP systems able to handle rapidly varying disturbances and transients. Examples include DP in ice, anchor handling operations, subsea pipe laying, automatic docking and DP while interacting with other fixed or floating structures. In recent years, several observers and controllers that improve the transient DP performance have been proposed. An effective approach is to use velocity measurements in the observer. However, high-quality velocity measurements are usually not available from Global Navigation Satellite System (GNSS) receivers at low speeds, which is the primary speed domain for most DP operations. Utilizing acceleration measurements from an inertial measurement unit (IMU) is another effective approach, this has been proposed for use in DP system by GNSS-aided inertial navigation [3], acceleration feedforward [4], and a hybrid observer switching between a model-based and inertial observer [5]. Other proposed approaches are implemented purely in software, and thus avoid the installation of expensive additional sensors, such as NPO with time-varying observer gains [6], and the resetting observer of [7]. The latter has inspired our approach, where the idea is to reset the state estimates if the output estimation error exceeds a predefined bound. The concept of *finite-time observers* (FTOs) appears to be a promising candidate for calculating the estimated state after a reset in a resetting observer. The FTO concept is that for an observable linear system, two Luenberger observers can be designed. By comparing the outputs of these observers, the exact system state can be calculated. FTOs first appeared in the literature in [8]. There, a continuous-time observer for a linear time-invariant (LTI) system was developed using time delays. Later, [9] designed an FTO for LTI systems that corrects the state estimate at a predetermined time after startup.

In this brief, we propose a hybrid observer design that combines the idea of the resetting mechanism of [7], where a reset is triggered if the estimation error exceeds predefined bounds, with an FTO approach for calculating the corrected state estimates after a reset. The FTO concept is extended to cover linear time-varying (LTV) systems, and an observer for

Manuscript received 13 October 2022; revised 21 May 2023; accepted 29 October 2023. Date of publication 21 November 2023; date of current version 25 April 2024. This work was supported in part by the Research Council of Norway through the Centers of Excellence Funding Scheme under Project 223254-NTNU AMOS, in part by the KPN ORCAS Project under Project 280655, and in part by the Air Force Office of Scientific Research under Grant FA9550-21-1-0452. Recommended by Associate Editor E. Zergeroglu. *(Corresponding author: Tobias R. Torben.)*

Tobias R. Torben and Roger Skjetne are with the Center for Autonomous Marine Operations (AMOS), Department of Marine Technology, Norwegian University of Science and Technology (NTNU), 7052 Trondheim, Norway (e-mail: tobias.torben@ntnu.no; roger.skjetne@ntnu.no).

Andrew R. Teel is with the Institute of Electrical and Electronics Engineers, University of California, Santa Barbara (UCSB), Santa Barbara, CA 93106 USA (e-mail: teel@ucsb.edu).

Øivind K. Kjerstad is with the Department of Ocean Operations and Civil Engineering, Norwegian University of Science and Technology (NTNU), 7052 Trondheim, Norway (e-mail: oivind.k.kjerstad@ntnu.no).

Emilie H. T. Wittemann is with TechnipFMC, 1366 Lysaker, Norway (e-mail: emiliewittemann@gmail.com).

Digital Object Identifier 10.1109/TCST.2023.3331338

generic LTV systems is developed. We then show how this observer can be applied for DP in a case study including simulations, a sensitivity analysis, and model scale experiments.

The brief is outlined as follows. First, some mathematical preliminaries on LTV systems and hybrid dynamical systems are given in Section II. In Section III, the novel observer design is developed and its stability is analyzed using hybrid dynamical systems theory. In Section IV the resetting observer is applied to a DP system and results from numerical simulations and model scale experiments are presented and analyzed. Some technical aspects of the approach are discussed in Section V with suggestions for further work, before concluding remarks are given in Section VI.

II. Preliminaries

A. Notation

In this brief, $\|\cdot\|$ denotes the Euclidean vector norm (two-norm), and $|\cdot|$ denotes the scalar absolute value. $\|x\|_{\mathcal{A}}$ denotes the distance from the vector x to the set $\mathcal{A}$, that is, $\|x\|_{\mathcal{A}} := \inf_{y\in\mathcal{A}} \|x - y\|$. Set-valued mappings are denoted by double arrows, for instance, $M : A \rightrightarrows B$ denotes a mapping M which maps values in A to subsets of B. The domain of a mapping is denoted $\mathrm{dom}(\cdot)$. The Cartesian product of A and B is denoted $A \times B$. $\lfloor\cdot\rfloor$ is the floor operator. $\kappa(\cdot)$ denotes the two-norm condition number for inversion. x^+ denotes the value of x after a discrete jump.

B. LTV Systems

We consider LTV systems of the form

$$\dot{z} = A(t)z + B(t)u(t) + \Lambda(t)d(t) \tag{1}$$

$$y = C(t)z \tag{2}$$

where for each $t \geq 0$, the state $z(t) \in \mathbb{R}^n$, the output $y(t) \in \mathbb{R}^p$, the input $u(t) \in \mathbb{R}^m$, and the disturbance $d(t) \in \mathbb{R}^q$. We assume $u(\cdot)$, $d(\cdot)$, and the matrices $A(\cdot)$, $B(\cdot)$, $C(\cdot)$, and $\Lambda(\cdot)$ are continuous and bounded functions. Under these conditions, a unique solution to (1) and (2) exists and is defined for all time [10].

We introduce the notion of exponential stability and present an important stability result for LTV systems, which will be used in the stability analysis in Section III-F. The following theorem guarantees the existence of a quadratic, time-varying Lyapunov function for uniformly globally exponentially stable (UGES) LTV systems.

Theorem 1 (Existence of a Quadratic Lyapunov Function [11]): Let $x = 0$ be the exponentially stable equilibrium point of $\dot{x} = A(t)x$, i.e., there exist $k > 0$ and $\lambda > 0$ such that $\|x(t)\| \leq k\|x(t_0)\| \exp(-\lambda(t-t_0))$, $\forall t \geq t_0 \geq 0$. Suppose also that $A(\cdot)$ is continuous and bounded. Let $Q(\cdot)$ be a continuous, bounded, symmetric, and uniformly positive definite matrix. Then, there exists a continuously differentiable, bounded, symmetric, and uniformly positive definite matrix $P(\cdot)$ that satisfies

$$-\dot{P}(t) = P(t)A(t) + A(t)^\top P(t) + Q(t). \tag{3}$$

Hence, $V(x,t) = x^\top P(t)x$ is a Lyapunov function for the system for which there exist positive constants k_1, k_2, and k_3 such that

$$k_1\|x\|^2 \leq V(x,t) \leq k_2\|x\|^2 \quad \forall x \in \mathbb{R}^n \quad \text{and} \quad t \geq 0 \tag{4}$$

$$\dot{V}(x,t) = \frac{\partial V(x,t)}{\partial t} + \frac{\partial V(x,t)}{\partial x}A(t) \leq -k_3\|x\|^2 \quad \forall x \in \mathbb{R}^n \quad \text{and} \quad t \geq 0. \tag{5}$$

C. Hybrid Dynamical Systems

To formulate the resetting observer equations and do a formal analysis, the *hybrid dynamical systems* framework of [12] is used. Only the main concepts and the results needed in our analysis are presented here. The reader is referred to [12] and [13], and references therein, for further details.

In this framework, the solution to a hybrid system is denoted $x(t, j)$, where $t \in \mathbb{R}_{\geq 0}$ is continuous time and $j \in \mathbb{N}$ is discrete time. The solutions are defined over *hybrid time domains*, formally defined in [12]. A hybrid dynamical system, $\mathcal{H} = (\mathcal{C}, F, \mathcal{D}, G)$, is modeled as a *constrained differential inclusion* and a *constrained difference inclusion*

$$x \in \mathcal{C} \quad \dot{x} \in F(x) \tag{6a}$$

$$x \in \mathcal{D} \quad x^+ \in G(x). \tag{6b}$$

When the state $x(t, j)$ is in the *flow set* $\mathcal{C}$, it evolves continuously (flows) according to the *differential inclusion* $\dot{x}(t, j) \in F(x(t, j))$. When $x(t, j)$ is in the *jump set* $\mathcal{D}$, it evolves discretely (jumps) according to the *difference inclusion* $x(t, j + 1) \in G(x(t, j))$.

Next, we define the notion of uniform global pre-exponential stability (UGpES) for hybrid systems.

Definition 1 (UGpES [14]): Given a hybrid dynamical system $\mathcal{H}$, a nonempty set $\mathcal{A} \subset \mathbb{R}^n$ is said to be globally pre-exponential stable (UGpES) of there exists positive constants c_1 and c_2 such that each solution x to $\mathcal{H}$ satisfies

$$\|x(t, j)\|_{\mathcal{A}} \leq c_1 \exp(-c_2(t + j))\|x(0, 0)\|_{\mathcal{A}} \quad \forall (t, j) \in \mathrm{dom}(x). \tag{7}$$

The term preexponential as opposed to exponential stability permits maximal solutions that are not complete.

III. Resetting Observer Design

A. Problem Statement

Consider an LTV system of the form given in (1) and (2). The objective of this brief is to calculate a state estimate $\hat{z}$, knowing the input $u(t)$, and given measurements of the output $y(t)$. It is assumed nominally that the external disturbance $d(t) = 0$, $\forall t \geq 0$. This assumption may seem contradictory, as a key motivation for the observer design is increased reactivity to unmodeled disturbances. However, the following developments will show that the unmodeled disturbances can be added as internal states that are effectively estimated by the observer. Furthermore, it can be assumed that these states are constant in the model used by the observer, thereby removing the external excitation $d(t)$. The model used in the observer design is thus reduced to

$$\dot{z} = A(t)z + B(t)u \tag{8}$$

$$y = C(t)z. \tag{9}$$

We first derive how an exact state estimate for an LTV system can be obtained from two Luenberger observers. Then we propose how to use this result in a hybrid resetting observer.

B. FTO Equations for LTV Systems

Consider two Luenberger observers for (8) and (9) with state estimates $z_i, i \in \{1, 2\}$, and dynamics

$$\dot{z}_i = A(t)z_i + B(t)u + L_i(t)(y - C(t)z_i) \tag{10}$$

where $L_i(t) \in \mathbb{R}^{n\times p}$ is a piecewise continuous and bounded injection gain matrix. Define $A_i(t) := A(t) - L_i(t)C(t)$ and the error variables $e_i := z - z_i$, and let $L_i(t)$ be chosen such that the origin is UGES for the error dynamics

$$\dot{e}_i = \dot{z} - \dot{z}_i = A_i(t)e_i \tag{11}$$

for $i \in \{1, 2\}$. The solutions for these systems can be expressed in terms of the state transition matrix Φ_i [10], according to

$$e_i(t) = \Phi_i(t, t_0)e(t_0). \tag{12}$$

We seek to calculate the true system state, z, at times $t_{k+1} > t_k > \cdots > t_0 \geq 0$ to enable the observer to reset the state estimates to z. At the start of each interval $[t_k, t_{k+1}]$, the two observers are initialized with the same state estimates, that is, $z_1(t_k) = z_2(t_k)$. The initial estimation error, $e(t_k)$ is thus equal for both observers, which implies that (12) can be used to set up two vectorial equations with two unknowns, $e(t_k)$ and $z(t_{k+1})$

$$\Phi_1(t_{k+1}, t_k)e(t_k) = z(t_{k+1}) - z_1(t_{k+1}) \tag{13}$$

$$\Phi_2(t_{k+1}, t_k)e(t_k) = z(t_{k+1}) - z_2(t_{k+1}). \tag{14}$$

Solving (13) for $e(t_k)$ yields

$$e(t_k) = \Phi_1^{-1}(t_{k+1}, t_k)(z(t_{k+1}) - z_1(t_{k+1})). \tag{15}$$

Inserting this into (14) and solving for the true system state, $z(t_{k+1})$ then yields

$$z(t_{k+1}) = \left(I - \Phi_2(t_k, t_{k+1})\Phi_1^{-1}(t_k, t_{k+1})\right)^{-1} \times \begin{bmatrix} -\Phi_2(t_k, t_{k+1})\Phi_1^{-1}(t_k, t_{k+1}) & I \end{bmatrix} \begin{bmatrix} z_1(t_{k+1}) \\ z_2(t_{k+1}) \end{bmatrix}. \tag{16}$$

Hence, if $\Phi_1(t_k, t_{k+1})$ and $I - \Phi_2(t_k, t_{k+1})\Phi_1^{-1}(t_k, t_{k+1})$ are invertible matrices, the true system state can be calculated from the state estimates $z_1(t_{k+1})$ and $z_2(t_{k+1})$. The calculated value of the true system state will be used to update the state estimates after a reset.

C. Calculating the State Transition Matrices

Section III-B shows that we need to know the value of the state transition matrices, $\Phi_1(t_{k+1}, t_k)$ and $\Phi_2(t_{k+1}, t_k)$, to calculate the true system state at a reset. For a generic LTV system, a closed-form expression of the state transition matrix rarely exists. Also, if the time dependence is driven by an external signal, the signal may not be known in advance. Here, we show how the state transition matrix can be numerically calculated online in an observer.

Consider a generic LTV system $\dot{x} = F(t)x$ which satisfies the conditions for existence and uniqueness given in Section II-B. Its solution is given by

$$x(t) = \Phi(t, t_0)x(t_0), \quad t \geq t_0 \geq 0 \tag{17}$$

where $\Phi(t, t_0)$ is the state transition matrix. It is trivial to show that $\Phi(t, t_0)$ is governed by the matrix differential equation

$$\dot{\Phi}(t, t_0) = F(t)\Phi(t, t_0). \tag{18}$$

Also, $\Phi(t_0, t_0) = I$, where $I \in \mathbb{R}^{n\times n}$ is the identity matrix. Therefore, the value of $\Phi(t, t_0)$ can be approximated online by numerically integrating (18) with initial condition $\Phi(t_0, t_0) = I$.

D. Design Considerations

A reset is triggered if the output estimation error exceeds predefined bounds. Let the error bounds be given by $\epsilon \in \mathbb{R}^p_{>0}$. A jump is triggered if $|(y - C(t)z_1)_i| \geq \epsilon_i$ for some $i \in \{1, 2, \ldots, p\}$. The error bounds should be chosen such that measurement noise does not trigger a jump.

The state estimate z_1 is used as the output of the observer. The variable z_2 is included only to accommodate an FTO state reset. The matrix $L_1(t)$ should therefore be tuned in the normal relaxed manner, to avoid measurement noise propagating into the state estimates. The matrix $L_2(t)$ should be tuned more aggressively such that the state estimates converge faster to measurements at the cost of less measurement noise filtering. Because a nonaggressive observer is used during steady-state conditions, and a jump is triggered only in the transient of a disturbance, this design gives the observer a "low gain - high reactivity" property, which is our aim.

State resets need to be separated by some dwell time in order for the FTO mechanism to robustly calculate corrected state estimates. The manifestation of this is that the condition number of $(I - \Phi_2(t_k, t_{k+1})\Phi_1^{-1}(t_k, t_{k+1}))$ will grow large as $t_{k+1} - t_k \to 0$, which gives numerical issues when calculating its inverse. On the other hand, the integral of the state transition matrices of (18) should be reset frequently to avoid modeling errors and disturbances causing drift in the state transition matrices resulting in inaccurate state resets. To control the timing of the jumps, we propose to always reset the state transition matrix integrals after a constant time interval δ. That is, they are reset at times $t_{k+1} > t_k > \cdots > t_0 \geq 0$, where $t_{k+1} = t_k + \delta$. The state transition matrices are reset to the identity matrix and z_2 is reset to the value of z_1, such that the two observers are initialized with the same estimation error before the next interval. A state reset in the output estimate, z_1, is triggered only if $|(y - C(t)z_1)_i| \geq \epsilon_i$ for some $i \in \{1, 2, \ldots, p\}$. Otherwise, z_1 is kept unchanged after the reset. Also, because conditions that ensure nonsingularity of $(I - \Phi_2(t_k, t_{k+1})\Phi_1^{-1}(t_k, t_{k+1}))$ for all times are not established for generic LTV systems, we propose to jump the output state estimate, z_1, only if the condition number of $(I - \Phi_2(t_k, t_{k+1})\Phi_1^{-1}(t_k, t_{k+1}))$ is sufficiently low. This is discussed further in Section V.

As shown in Section III-B, the FTO approach will reset the state estimates exactly to the true values of the states in the

nominal case, and therefore improve the transient performance. As noted in Section III-A, if the system is expected to be subject to severe unmodeled disturbances, it may be beneficial to add the disturbances as states to be estimated by the observer. Furthermore, it can be assumed that these states are constant in the model used by the observer. Every δ seconds, the resetting mechanism will check if $|(y - C(t)z_1)_i| \geq \epsilon_i$ for some $i \in \{1, 2, \ldots, p\}$. If this is the case, the system is likely subject to an unmodeled disturbance and a reset of the state estimates will occur using the FTO approach. Equation (16) will then calculate the correct magnitude for a constant disturbance acting over the previous δ seconds and update the disturbance state estimates accordingly. Hence, adding the disturbance as a state enables the resetting observer to be effective also when subject to severe disturbances.

Finally, our experience has shown that resetting to the true system state may cause overshooting behavior after a reset due to measurement noise and disturbances causing inaccuracies in the FTO estimates. To address this challenge, we propose to add a tunable linear interpolation to the jump map. That is, instead of jumping directly to the z value computed by (16), the system jumps to $kz + (1 - k)z_1$, where $k \in [0, 1]$ is a tunable scalar.

E. Hybrid Observer Equations

We are now ready to state the hybrid observer equations for the resetting observer using the hybrid dynamical systems framework introduced in Section II-C.

We begin by defining the state variables of the hybrid system. Let z be the true system state, which is assumed to live in a compact set $\mathbb{K} \subset \mathbb{R}^n$. The state estimates z_1 and z_2 live in $\mathbb{R}^n$. The state transition matrices for the Luenberger observer error dynamics Φ_1 and Φ_2 are governed by (18), and will thus have no finite escape times. Also, since they are periodically reset to identity, these matrices will live in a compact set $M \subset \mathbb{R}^{n\times n}$. The variable ζ is a scalar timer for the resets, and τ is the time variable. In total, the state of the hybrid system is defined as

$$\begin{aligned} x &= (z, z_1, z_2, \Phi_1, \Phi_2, \zeta, \tau) \\ &\in \mathbb{K} \times \mathbb{R}^n \times \mathbb{R}^n \times M \times M \times \mathbb{R}_{\geq 0} \times \mathbb{R}_{\geq 0}. \end{aligned} \tag{19}$$

Following the developments of Section III, the flow map is expressed as the set-valued mapping

$$\dot{x} \in F(x) := \bigcup_{u\in\mathbb{U}} f(x, u) \tag{20}$$

where $\mathbb{U}$ is a compact subset of $\mathbb{R}^m$ and

$$f(x, u) := \begin{bmatrix} A(\tau)z + B(\tau)u \\ A_1(\tau)z_1 + B(\tau)u + (A(\tau) - A_1(\tau))z \\ A_2(\tau)z_2 + B(\tau)u + (A(\tau) - A_2(\tau))z \\ A_1(\tau)\Phi_1 \\ A_2(\tau)\Phi_2 \\ 1 \\ 1 \end{bmatrix}. \tag{21}$$

The jump map is defined as

$$x^+ = g(x) := \begin{bmatrix} z \\ h(x) \\ h(x) \\ I \\ I \\ 0 \\ \tau \end{bmatrix} \tag{22}$$

where

$$h(x) := \begin{cases} k\Psi(x)\begin{bmatrix} z_1 \\ z_2 \end{bmatrix} + (1 - k)z_1; \\ \quad \text{if } |Cz_1 - y|_i \geq \epsilon_i, \\ \quad \text{for some } i \in \{1, 2, \ldots, p\} \text{ and} \\ \quad \kappa\left(I - \Phi_2\Phi_1^{-1}\right) \leq c_{\max} \\ z_1; \quad \text{otherwise} \end{cases} \tag{23}$$

for $k \in [0, 1]$ and

$$\Psi(x) := \left(I - \Phi_2\Phi_1^{-1}\right)^{-1}\left[-\Phi_2\Phi_1^{-1} \quad I\right]. \tag{24}$$

The threshold $c_{\max} \in \mathbb{R}_{\geq 1}$ is the highest value of the condition number of $I - \Phi_2\Phi_1^{-1}$ for which a reset using Ψ can occur.

The flow set is defined as

$$\mathcal{C} := \mathbb{K} \times \mathbb{R}^n \times \mathbb{R}^n \times M \times M \times [0, \delta] \times \mathbb{R}_{\geq 0} \tag{25}$$

and the jump set is defined as

$$\mathcal{D} := \mathbb{K} \times \mathbb{R}^n \times \mathbb{R}^n \times M \times M \times \{\delta\} \times \mathbb{R}_{\geq 0}. \tag{26}$$

This completely defines the hybrid system $\mathcal{H} = (\mathcal{C}, F, \mathcal{D}, g)$.

F. Formal Stability Analysis

The following stability result gives sufficient conditions for establishing UGpES of the resetting observer error dynamics.

Theorem 2: For the resetting observer $\mathcal{H}$ defined by (20)–(26), let $u(\cdot)$, $A(\cdot)$, $B(\cdot)$, $C(\cdot)$, $L_1(\cdot)$, and $L_2(\cdot)$ be continuous and bounded functions, and let $L_i(\cdot)$, $i \in 1, 2$, be chosen such that $e_i = 0$ for (11) is UGES. Furthermore, let $\delta > 0$ and $k \in [0, 1]$. Then, the set $\mathcal{A} := \{(z, z_1) \in \mathbb{K} \times \mathbb{R}^n : z = z_1\} \times \mathbb{R}^n \times M \times M \times [0, \delta] \times \mathbb{R}_{\geq 0}$ is UGpES for $\mathcal{H}$.

Proof: First we note that $\|x\|_{\mathcal{A}} = \|z - z_1\| = \|e_1\|$ since z_2, Φ_1, Φ_2, ζ, and τ are always in their respective subsets of $\mathcal{A}$ by construction. We also note that the time dependence of the LTV system has been replaced by the time state, τ, in the hybrid system. Because the error dynamics of e_1 are governed by the UGES LTV system $(de_1/d\tau) = A_1(\tau)e_1$, Theorem 1 implies that there exist $Q(\cdot)$, $P(\cdot)$, and $V(e_1, \tau) := e_1^\top P(\tau)e_1$ that satisfy (4) and (5) when $\mathcal{H}$ is evolving continuously. Using the upper bound in (4) we can turn (5) into

$$\dot{V}(e_1, \tau) \leq -\frac{k_3}{k_2}V(e_1, \tau). \tag{27}$$

Then, using a standard comparison theorem (e.g., Lemma 3.4 from [11]) we get that for each (s, j), (t, j) in the domain

of the solution with $t > s$, we have

$$V(e_1(t,j),\tau(t,j)) \le \exp\left(-\frac{k_3}{k_2}(t-s)\right)V(e_1(s,j),\tau(s,j)). \tag{28}$$

Using both the lower bound and the upper bound from (4) we get

$$k_1\|e_1(t,j)\|^2 \le \exp\left(-\frac{k_3}{k_2}(t-s)\right)k_2\|e_1(s,j)\|^2. \tag{29}$$

Dividing both sides by k_1 and taking square roots we arrive at the following exponentially decreasing bound when $\mathcal{H}$ is evolving continuously:

$$\|e_1(t,j)\| \le \sqrt{\frac{k_2}{k_1}}\exp\left(-\frac{k_3}{2k_2}(t-s)\right)\|e_1(s,j)\|. \tag{30}$$

If $\|e_1\|$ is nonincreasing at jumps, that is, for each (t,j), $(t,j+1)$ in the domain of the solution we have

$$\|e_1(t,j+1)\| \le \|e_1(t,j)\| \tag{31}$$

then it follows from (30), that, for each $(s,i),(t,j)$ in the domain of the solution with $s+i < t+j$ we have

$$\|e_1(t,j)\| \le \sqrt{\frac{k_2}{k_1}}\exp\left(-\frac{k_3}{2k_2}(t-s)\right)\|e_1(s,i)\|. \tag{32}$$

We show that $\|e_1\|$ is nonincreasing at jumps next. From (23) we have that

$$e_1^+ = e_1 \tag{33}$$

or

$$e_1^+ = z^+ - z_1^+ = z - \left(k\Psi(x)\begin{bmatrix}z_1\\ z_2\end{bmatrix} + (1-k)z_1\right). \tag{34}$$

In the first case, $\|e_1\|$ is trivially nonincreasing. In the second case, we have that $\Psi(x)\left[\begin{smallmatrix}z_1\\ z_2\end{smallmatrix}\right] = z$, as shown in Section III-B. It follows that:

$$e_1^+ = z - (z_1 + k(z - z_1)) = (1-k)e_1. \tag{35}$$

Hence,

$$\|e_1^+\| = (1-k)\|e_1\| \le \|e_1\| \tag{36}$$

since $k \in [0,1]$. Hence, $\|e_1\|$ is always nonincreasing at jumps and (32) holds for $\mathcal{H}$.

The bound in (32) shows that $\|e_1\|$ is exponentially decreasing when t grows. In order to satisfy the definition of UGpES in (7), we need to show that e_1 is exponentially decreasing when $t+j$ grows. To achieve this, we will find a $\mathcal{K}_\infty$ function $\alpha(\cdot)$ such that $t \ge \alpha(t+j)$, and replace t with $\alpha(t+j)$ in (30). Since jumps are always separated by $\delta > 0$ time units, due to the construction of $\mathcal{C}$ and $\mathcal{D}$ and the fact that $\zeta^+ = 0$ and $\dot\zeta = 1$, we have that

$$j = \left\lfloor \frac{t}{\delta}\right\rfloor \le \frac{t}{\delta} \implies t \ge \delta j. \tag{37}$$

Adding δt to both sides of the inequality gives

$$\delta t + t \ge \delta j + \delta t \implies t(1+\delta) \ge \delta(t+j). \tag{38}$$

Rearranging terms, we arrive at the $\mathcal{K}_\infty$ relation

$$t \ge \frac{\delta}{1+\delta}(t+j). \tag{39}$$

Replacing t with $(\delta/(1+\delta))(t+j)$ in (32) with $(s,i) = (0,0)$ gives the desired bound

$$\begin{aligned}\|e_1(t,j)\| &\le \sqrt{\frac{k_2}{k_1}}\exp\left(-\frac{k_3}{2k_2}t\right)\|e_1(0,0)\|\\ &\le \sqrt{\frac{k_2}{k_1}}\exp\left(-\frac{k_3\delta}{2k_2(1+\delta)}(t+j)\right)\|e_1(0,0)\|.\end{aligned} \tag{40}$$

Hence, (40) satisfies the definition of UGpES in (7) with $c_1 = ((k_2/k_1))^{1/2} > 0$ and $c_2 = (k_3\delta/(2k_2(1+\delta))) > 0$. ■

IV. Case Study: DP

The resetting observer of (20)–(26) applies to generic observable LTV systems. In this section, we show how it can be applied to a DP system.

A. Mathematical Modeling and Observer Design

The standard control design model for the low-frequency motion of a marine surface is defined as

$$\dot\eta = R(\psi)\nu \tag{41a}$$
$$\dot b = d(t) \tag{41b}$$
$$M\dot\nu + D\nu = \tau + R(\psi)^\top b \tag{41c}$$
$$y = \eta \tag{41d}$$

where $\eta \in \mathbb{R}^3$ is the position and heading, $\nu \in \mathbb{R}^3$ is the body frame velocity and turn rate, $b \in \mathbb{R}^3$ is a bias load, $d(t) \in \mathbb{R}^3$ is the disturbance, and $\tau \in \mathbb{R}^3$ compiles the body frame thruster forces. $R(\psi) \in \mathbb{R}^{3\times3}$ is a three degree of freedom rotation matrix, $M \in \mathbb{R}^{3\times3}$ is the mass matrix, including added mass, and $D \in \mathbb{R}^{3\times3}$ is the linear damping matrix.

The system of (41) is a highly simplified control design model which attempts to capture the main dynamics of the complex hydrodynamic interactions between the vessel, thrusters, and water. In this model, the bias state is used as an internal state to estimate unmodeled loads, and in the observer model it will be assumed that $d(t) = 0$, as suggested in Section III-D. Equation (41) is a nonlinear model due to the rotation matrices. However, since the heading is measured by a gyrocompass within the compact interval of $[-\pi,\pi]$ and the heading rate (its derivative) is bounded due to vessel damping and limited thruster forces, we can use the heading measurement directly in the rotation matrix as an external time signal and assuming $R(t) := R(\psi(t))$ to be a time-varying matrix [15]. The nonlinear system of (41) can then be written in LTV form as

$$z = \left[\eta^\top, b^\top, \nu^\top\right]^\top \in \mathbb{R}^9, \quad u = \tau \in \mathbb{R}^3 \tag{42a}$$
$$\dot z = A(t)z + Bu \tag{42b}$$
$$y = Cz \tag{42c}$$
$$A(t) = \begin{bmatrix}0_{3\times3} & 0_{3\times3} & R(t)\\ 0_{3\times3} & 0_{3\times3} & 0_{3\times3}\\ 0_{3\times3} & M^{-1}R(t)^\top & -M^{-1}D\end{bmatrix} \tag{43}$$

TABLE I
PARAMETER VALUES USED IN THE SIMULATION STUDY

Parameter	Value
Differential GNSS standard deviation	$0.1m$
Dual-band GNSS standard deviation	$1.5m$
Heading sensor standard deviation	0.3°
Sensor Gauss-Markov time constant $(1/c)$	$1100s$
Sensor sample time (T_s)	$1.0s$
Notch filter central frequency (ω_0)	$1.0rad/s$
Notch filter bandwidth (ω_c)	$0.5rad/s$
Reset time (δ)	$2.5s$
Interpolation gain (k)	0.7
Estimation error bounds (ϵ)	$[0.5m, 0.5m, 0.05rad]$
Process covariance for L_1 (Q_1)	$diag([50, 50, 10])$
Measurement covariance for L_1 (R_1)	$diag([15, 15, 1])$
Process covariance for L_2 (Q_2)	$10^{-7}Q_1$
Measurement covariance for L_2 (R_2)	R_1

$$B = \begin{bmatrix} 0_{3\times3} \\ 0_{3\times3} \\ M^{-1} \end{bmatrix} \tag{44}$$

$$C = \begin{bmatrix} I_{3\times3} & 0_{3\times3} & 0_{3\times3} \end{bmatrix}. \tag{45}$$

Luenberger observers for z_1 and z_2 can then be designed as

$$\dot{z}_i = A(t)z_i + Bu + L_i(t)(y - Cz_i) \tag{46}$$

where

$$L_i(t) = \begin{bmatrix} K_{1,i} \\ K_{2,i} \\ M^{-1}R^\top(t)K_{3,i} \end{bmatrix} \in \mathbb{R}^{9\times3} \tag{47}$$

such that the origin is UGES for $\dot{e}_i = A_i(t) := A(t) - L_i(t)C$. These Luenberger observers can now readily be used in the resetting observer of (20)–(26).

B. Simulation Study

To evaluate the performance of the proposed observer design, it was tested in simulation with a high-fidelity simulation model. The model used is the *Supply Vessel* from marine systems simulator [16]. The parameter values used in the simulation study are given in Table I.

The measurement errors of the GNSS east and north components and heading sensor are modeled as Gauss-Markov processes [17], that is,

$$v[n+1] = e^{-cT_s}v[n] + \rho[n] \tag{48}$$

where $v[n]$ is the measurement at discrete time n, $(1/c)$ is the time constant for the process, T_s is the sampling time and ρ is zero-mean Gaussian white noise with standard deviation, σ. The values of c, T_s, and σ are chosen to match the characteristics of commercially available differential and dual-band GNSS and heading sensors. To remove wave-frequency components of the measurements, they are notch filtered before entering the observer. The notch filter used is a linear second-order filter with transfer function

$$H(s) = \frac{s^2 + \omega_0^2}{s^2 + \omega_c s + \omega_0^2} \tag{49}$$

where ω_0 is the central frequency and ω_c is the width of the rejected band. The injection gain matrices for the Luenberger observers, L_1 and L_2, were obtained using optimal gains from a linear Kalman filter design about zero heading. The L_1 gains were first calculated by tuning the process covariance matrix Q_1 and the measurement covariance matrix, R_1. Then, the more aggressive L_2 gains were calculated by keeping $R_2 = R_1$ while setting Q_2 to a significantly lower value of $10^{-7}Q_1$.

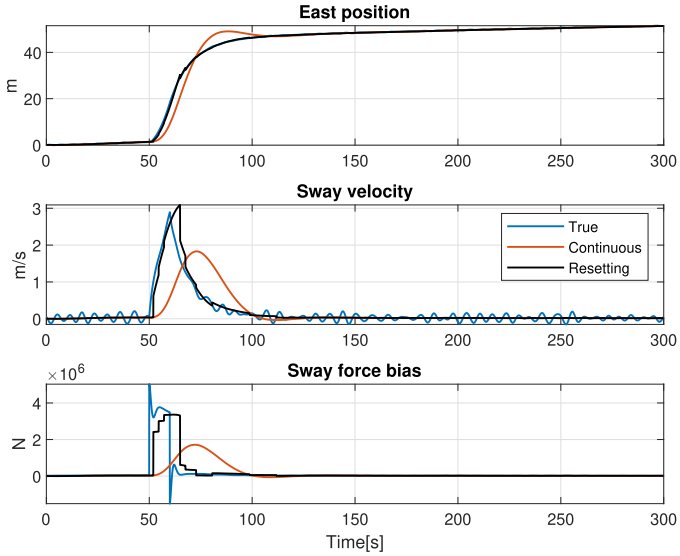

Fig. 1. Simulation results for evaluating transient and steady state performance.

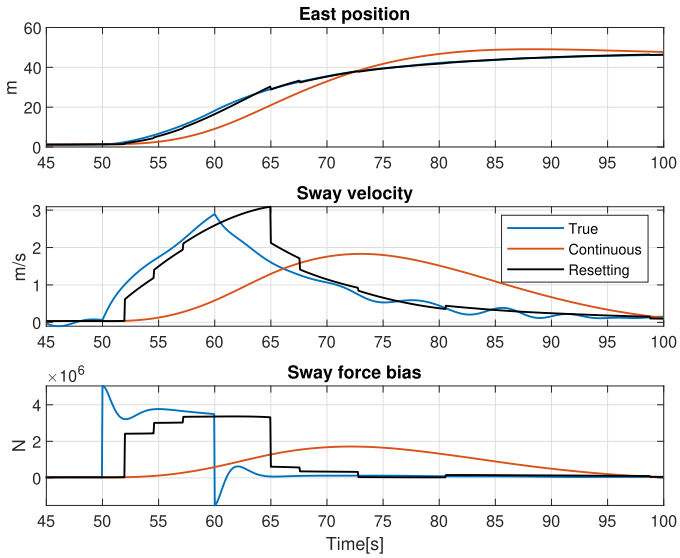

Fig. 2. Locally enlarged version of Fig. 1 around the transient phase.

1) Transient and Steady State Performance: As introduced in Section I, our motivation for this observer design is to achieve increased reactivity against rapidly changing disturbances without compromising the steady-state performance. To investigate whether the resetting observer accomplishes this goal, the vessel was excited by an impulsive sway disturbance with magnitude 5000 kN and duration 10 s at $t = 50$ s, followed by a long period of steady-state operation. The sea state in the simulation was governed by a Joint North Sea Wave Project (JONSWAP) wave spectrum [18] with significant wave height 2 m and peak period 6.3 s.

The results are presented in Figs. 1 and 2. The results marked "continuous" show state estimates from the NPO of [2], which is equivalent to the LTV Luenberger observer with innovation gain $L_1(t)$ in the resetting observer. The results show promising performance. The resetting observer gives a substantial improvement during the transient phase, without amplifying measurements noise or introducing wave frequency components to the state estimates. The vessel is subject to a severe disturbance, but this is captured well by the resetting mechanism in the bias estimate, which estimates a constant value for the bias for each δ interval. It can be seen that there is a substantial wave-frequency component in the sway velocity. However, since this measurement is notch-filtered before entering the observer, this does not trigger unwanted jumps. There is some delay in the state estimates of the resetting observer due to the resetting time δ and the phase lag introduced by the notch filter. When tuning the notch filter, there must be a trade-off between phase lag and wave attenuation. This should be adjusted to the prevailing sea state to ensure that the wave-frequency component of the measurements can not trigger jumps.

2) Sensitivity Analysis of Observer Parameters: To investigate the effect of varying the tunable parameters of the resetting mechanism, a sensitivity analysis was performed on the interpolation gain, k, reset time δ, and error bounds ϵ. To obtain an objective and quantitative measure of the observer performance in a simulation, a key performance indicator (KPI) was developed based on the estimation error. In order to combine variables with different physical units in the same KPI, all variables were nondimensionalized using the BIS system [18]. The KPI, J_{tot} is defined by

$$J_{\text{tot}} = \int_0^T \left\| z_{\text{bis}}(t) - \hat{z}_{\text{bis}}(t) \right\| dt \tag{50}$$

where T is the length of the simulation. Estimated state variables, obtained from z_1 of the resetting observer, are denoted by hatted symbols. Lower values of the KPI indicate better observer performance.

A total of 100 simulations were run for each of the tuning parameters k, δ, and ϵ, where their values were varied within a predefined range. The other parameters were kept unchanged at the values given in Table I. To investigate the relationship between measurement noise and tuning parameters, the sensitivity analysis was conducted both with a differential and a dual-band GNSS model. Each simulation had a duration $T = 1000$ s, where the vessel was subject to both impulsive and slowly varying disturbances in surge, sway, and yaw followed by a longer period of steady-state operation with only wave and measurement noise disturbances. The disturbances induced simultaneous heading and surge/sway motion, thereby exciting the time-varying (nonlinear) dynamics of the system.

First, the effect of the interpolation gain k is studied for values in the interval [0, 1], which is the entire allowable range for k. Using $k = 0$ is equivalent to a continuous-time NPO observer, completely disregarding the FTO estimates, while for $k = 1$ we use the FTO estimates directly after a reset. The top plot in Fig. 3 shows the trend that the performance improves as k is increased, and performance is drastically improved compared to the NPO score at $k = 0$. The improvement flattens out for higher values of k. As we discussed in Section III-D, having too high values of k may lead to overshoots after a reset due to inaccuracies caused by measurement noise and unmodeled disturbances, and it is therefore more advantageous to do several more gradual jumps by using a lower value of k. The results of Fig. 3 underpins this theory, as the simulations with higher measurement noise (dual-band) perform worse for high-values of k. Our choice of using $k = 0.7$ appears to find a good balance.

Next, the effect of varying the reset time δ is studied. The middle plot of Fig. 3 shows the trend that the performance decreases as the reset time increases. This is as expected since a higher reset time means that the resetting mechanism must wait longer before it can reset to a more correct state estimate. More surprisingly, the resetting observer produces excellent state estimates also for very low values of δ. As noted in Section III-D, the condition number of $(I - \Phi_2\Phi_1^{-1})$ in the jump map grows large when δ is decreased. We have found that when δ approaches the time step size of the control system, which in this case was 0.05 s, the observer becomes unstable if we also disable the check on the condition number in the jump map. In these cases the condition number of $(I-\Phi_2\Phi_1^{-1})$ is of the order of 10^{16}. Since we are using double precision floating point arithmetic in the simulations, the machine epsilon is $\approx 10^{-16}$, meaning that the matrix is so ill-conditioned that numerical round-off error will be amplified to the degree that the results are useless. However, we found that when δ is greater than about three times the time step size, the observer works perfectly fine even though the condition number of $(I - \Phi_2\Phi_1^{-1})$ is of the order of 10^{10}. This indicates that the resetting observer design is highly robust against $(I-\Phi_2\Phi_1^{-1})$ being ill-conditioned. In all other simulations, $\delta = 2.5$ s is used. As Fig. 3 shows, there are no significant performance gains by using a lower δ than this. With $\delta = 2.5$ s the condition number of $(I - \Phi_2\Phi_1^{-1})$ has values around 50, giving large robustness margins before singularity becomes an issue.

Finally, the effect of varying the error bounds ϵ is investigated. In the other simulations, $\epsilon = [0.5\text{ m}, 0.5\text{ m}, 0.05\text{ rad}]$ was used. In the sensitivity analysis, scaled versions of this is used, that is, $\epsilon = c_\epsilon[0.1\text{ m}, 0.1\text{ m}, 0.01\text{ rad}]$, with $c_\epsilon \in [0.1, 10]$. The bottom plot in Fig. 3 shows that the performance is poor for very low values of ϵ. This occurs because measurement noise constantly triggers unwanted resets. This effect is more pronounced for the simulations with higher measurement noise (dual-band). Conversely, for high values of c_ϵ the performance is decreasing slightly with increasing ϵ due to lower reactivity when the error bounds are too big. The tuning used in the other simulations corresponds to a c_ϵ value of 5, which appears to find a good balance based on the results in Fig. 3.

An important finding from the sensitivity analysis is that the observer has good performance over a wide range of values for the tunable parameters of the resetting mechanism. Based on the results of the sensitivity analysis, we recommend that k should be reduced if there is high measurement noise. The value of δ should be chosen significantly larger than the time step of the control system and can generally be chosen much

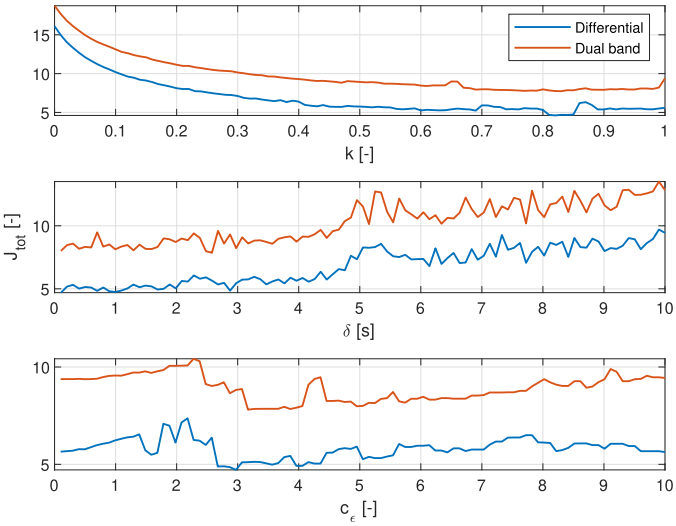

Fig. 3. Sensitivity analysis investigating effect of the tunable parameters k, δ, and ϵ on the KPI J_{tot}.

Fig. 4. Cybership III ship model in the MCLab wave tank.

larger than this without negatively impacting performance. The ϵ bounds should be set larger than the prevailing measurement noise.

C. Experimental Study

To validate the results from the simulation study, the resetting observer was tested experimentally in model scale experiments. The experiments were conducted in the Marine Cybernetics Laboratory (MC-Lab) wave tank at the Norwegian University of Science and Technology (NTNU), Trondheim, Norway. The test vessel used was Cybership III, a 1:30 scale model of an offshore supply vessel, as shown in Fig. 4. For more details on the experimental study, the reader is referred to [19]. This thesis includes more detailed experimental results and performs a comparison of the resetting observer with the NPO of [2] and the NPO with time-varying gains of [6]. The thesis compared the three observers in ten different simulated scenarios and five different experimental scenarios. The results were highly convincing of the merits of the resetting observer, showing that the resetting observer performed better than the NPO in all simulated and experimental scenarios, and it performed better than the NPO with time-varying gains in nine of ten simulated scenarios and all experimental scenarios.

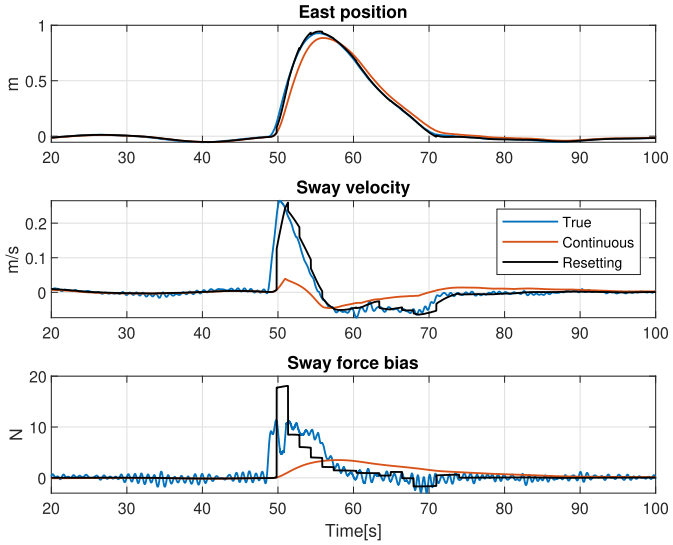

Fig. 5. Experimental results for the resetting observer.

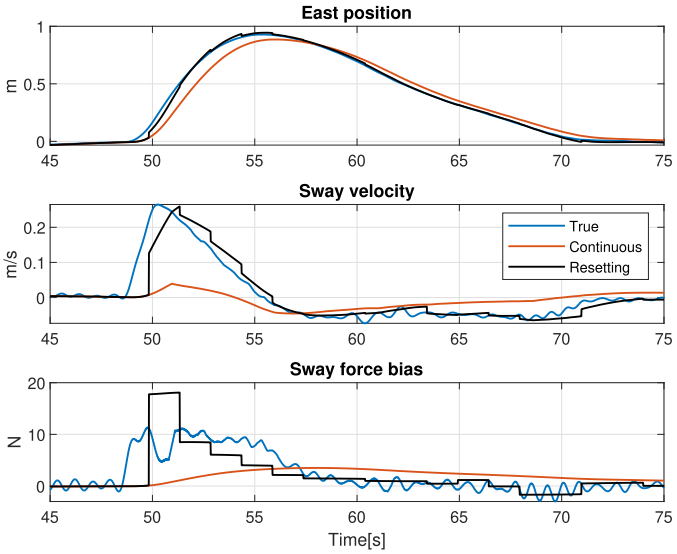

Fig. 6. Locally enlarged version of Fig. 5 around the transient phase.

In this brief, we give the results of one experimental scenario which is similar to the simulated scenario in Section IV-B1. This is achieved by giving the ship model a push in the sway direction, thereby exerting an impulse-like, unmodeled disturbance. A notable difference is that the observer was running in closed loop with a DP station-keeping controller in the experiments, thereby giving lower displacements than in the simulated scenario. The experiment was conducted in a moderate sea state, generated from a JONSWAP spectrum with significant wave height 0.04 m (1.2 m full-scale) and peak period 0.8 s (4.4 s full-scale). The results from the experiment are shown in Figs. 5 and 6. The results validate the findings in the simulation study by showing similar behavior and performance gain compared to a continuous-time observer. The results show that the peak of bias estimate from the resetting observer is higher than the estimated true bias signal. We believe this is an artifact of the

filtering used in the estimation of the true bias signal, which has filtered out the actual peak.

V. Discussion and Further Work

Our work does not include conditions to ensure nonsingularity of $(I - \Phi_2\Phi_1^{-1})$ for all times. Engel and Kreisselmeier [8] give sufficient, but highly conservative conditions for nonsingularity in the case of LTI systems. However, the extension of these conditions to the time-varying case is not trivial. The brief [20] proposes a workaround for this problem for uniformly observable systems LTV system by transformation to observer canonical form and separating out and canceling the time-varying dynamics resulting in time-invariant error dynamics. The state-transition matrix is thus the matrix exponential and nonsingularity $(I - \Phi_2\Phi_1^{-1})$ can therefore be established up front by inspection. This approach is, however, not attractive for the DP application because the transformation to observer canonical form requires signals that are not typically available in DP systems. In our work, we use a practical solution to avoid inverting a singular matrix by adding a check on the condition number of $(I - \Phi_2\Phi_1^{-1})$ before doing a jump, as stated in (22). In our experience, this has worked very well in practice. Our experience shows that despite the time-varying dynamics of the observer, the condition number stays practically constant throughout a simulation. The main factor influencing the condition number is the reset time δ. By running some simulations, the relationship between δ and the condition number of $(I - \Phi_2\Phi_1^{-1})$ can be established. This relationship can be used to find a safe value for δ. Combining this knowledge with the results showing that the observer is highly robust against ill-conditioned matrices and the check of condition number in the jump map, the singularity of $(I - \Phi_2\Phi_1^{-1})$ does not seem to be a likely problem in practice. Nevertheless, establishing a priori conditions for nonsingularity would be a valuable addition to the observer design, and we leave this for future work.

VI. Conclusion

We have presented a resetting observer for LTV systems. A reset is triggered if the output estimation error exceeds predefined bounds. To calculate corrected state estimates after a reset, an FTO approach is used. The FTO equations have been derived for LTV systems. The observer equations have been formulated in a hybrid dynamical systems framework, and sufficient conditions for UGpES have been given. The observer design has applications for DP of marine surface vessels. A case study for this application was conducted with numerical simulations and an experimental demonstration. The results showed promising results, with improved transient performance without compromising steady-state performance compared to the state-of-the-art continuous-time observer. These properties may enable DP operations in more challenging conditions, as well as better noise filtering properties due to the low injection gains. The resetting observer may also lower the requirements for model and parameter accuracy, as it more rapidly captures and corrects for model errors. The discussion highlights developing conditions that guarantee nonsingularity in the resetting mechanism as a topic for future research.

References

[1] A. J. Sørensen, "A survey of dynamic positioning control systems," *Annu. Rev. Control*, vol. 35, no. 1, pp. 123–136, Apr. 2011.

[2] T. I. Fossen and J. P. Strand, "Passive nonlinear observer design for ships using Lyapunov methods," *Automatica*, vol. 35, no. 1, pp. 3–16, 1999.

[3] T. H. Bryne, R. H. Rogne, T. I. Fossen, and T. A. Johansen, "A virtual vertical reference concept for aided inertial navigation at the sea surface," *Control Eng. Pract.*, vol. 70, pp. 1–14, Jan. 2018.

[4] Ø. K. Kjerstad and R. Skjetne, "Disturbance rejection by acceleration feedforward for marine surface vessels," *IEEE Access*, vol. 4, pp. 2656–2669, 2016.

[5] A. H. Brodtkorb, S. A. Værnø, A. R. Teel, A. J. Sørensen, and R. Skjetne, "Hybrid controller concept for dynamic positioning of marine vessels with experimental results," *Automatica*, vol. 93, pp. 489–497, Jul. 2018.

[6] S. A. Værnø, A. H. Brodtkorb, R. Skjetne, and V. Calabrò, "Time-varying model-based observer for marine surface vessels in dynamic positioning," *IEEE Access*, vol. 5, pp. 14787–14796, 2017.

[7] Ø. K. Kjerstad, "Dynamic positioning of marine vessels in level ice," Ph.D. thesis, Dept. Marine Technol., NTNU, Trondheim, Norway, 2016.

[8] R. Engel and G. Kreisselmeier, "A continuous-time observer which converges in finite time," *IEEE Trans. Autom. Control*, vol. 47, no. 7, pp. 1202–1204, Jul. 2002.

[9] T. Raff and F. Allgower, "An impulsive observer that estimates the exact state of a linear continuous-time system in predetermined finite time," in *Proc. Medit. Conf. Control Autom.*, Jun. 2007, pp. 2–4.

[10] C.-T. Chen, *Linear System Theory and Design*, 3rd ed. Oxford, U.K.: Oxford Univ. Press, 1999.

[11] H. K. Khalil, *Nonlinear Systems*, 2nd ed. Upper Saddle River, NJ, USA: Prentice-Hall, 2002.

[12] R. Goebel, R. G. Sanfelice, and A. R. Teel, *Hybrid Dynamical Systems: Modeling, Stability, and Robustness*. Princeton, NJ, USA: Princeton Univ. Press, 2012.

[13] R. Goebel, R. G. Sanfelice, and A. Teel, "Hybrid dynamical systems," *IEEE Control Syst. Mag.*, vol. 29, no. 2, pp. 28–93, Apr. 2009.

[14] R. G. Sanfelice, *Hybrid Feedback Control*. Princeton, NJ, USA: Princeton Univ. Press, 2021.

[15] S. A. Værnø, R. Skjetne, Ø. K. Kjerstad, and V. Calabrò, "Comparison of control design models and observers for dynamic positioning of surface vessels," *Control Eng. Pract.*, vol. 85, pp. 235–245, Apr. 2019.

[16] T. Perez, O. Smogeli, T. I. Fossen, and A. J. Sørensen, "An overview of the marine systems simulator (MSS): A simulink toolbox for marine control systems," *Model., Identificat. Control*, vol. 27, no. 4, pp. 259–275, 2006.

[17] R. W. Beard and T. W. McLeain, *Small Unmanned Aircraft: Theory and Practice*. Princeton, NJ, USA: Princeton Univ. Press, 2012.

[18] T. I. Fossen, *Handbook of Marine Craft Hydrodynamics and Motion Control*. Hoboken, NJ, USA: Wiley, 2011.

[19] E. H. T. Wittemann, "Master thesis: Hybrid observers for autonomous surface vessels experiencing varying operational conditions," M.S. thesis, Dept. Marine Technol., Norwegian Univ. Sci. Technol. (NTNU), Trondheim, Norway, 2021.

[20] P. H. Menold, R. Findeisen, and F. Allgower, "Finite time convergent observers for linear time-varying systems," in *Proc. 11th Medit. Conf. Control Autom.*, Dec. 2013, pp. 5673–5678.